

# Data report: high-resolution bulk density, dry density, and porosity records from the Arctic Coring Expedition, IODP Expedition 302<sup>1</sup>

Matt O'Regan<sup>2</sup>

## Chapter contents

<b>Abstract</b> .....	<b>1</b>
<b>Introduction</b> .....	<b>1</b>
<b>Methods</b> .....	<b>2</b>
<b>Results and discussion</b> .....	<b>3</b>
<b>Conclusions</b> .....	<b>4</b>
<b>Acknowledgments</b> .....	<b>4</b>
<b>References</b> .....	<b>4</b>
<b>Figures</b> .....	<b>5</b>
<b>Tables</b> .....	<b>10</b>

## Abstract

Sediments recovered from the Lomonosov Ridge during Integrated Ocean Drilling Program (IODP) Expedition 302, the Arctic Coring Expedition (ACEX), provide a unique archive of paleoenvironmental change in the central Arctic Ocean. High-resolution petrophysical data, acquired using the multisensor core logger (MSCL), comprise a valuable component of the data obtained from this sedimentary record. However, the nondestructive measurements performed using the MSCL are highly dependent on core quality and sensor calibration. Quality control on bulk density measurements from the MSCL is routinely provided by comparison with direct measurements of bulk density ( $\rho_B$ ) performed at coarser resolution on discrete samples. Here, results from these discrete analyses are used to correct  $\rho_B$  measurements from the MSCL. The method and rationale for these corrections are outlined in this study, and the corrected MSCL  $\rho_B$  records are presented. Using the corrected records, high-resolution dry density ( $\rho_D$ ) and porosity ( $\phi$ ) logs are generated, providing a means for determining mass accumulation rates and investigating lithology-dependent compaction processes in central Arctic Ocean sediments.

## Introduction

The Lomonosov Ridge is a sliver of continental crust that rifted from the Barents–Kara Sea margin at ~57 Ma (see the “[Expedition 302 summary](#)” chapter). Since the onset of rifting, >400 m of Cenozoic sediments have been deposited as the ridge drifted toward its present position in the center of the Arctic Ocean. The Arctic Coring Expedition (ACEX) targeted four sites located on the central Lomonosov Ridge along seismic Line AWI91090 (Fig. [F1](#)) (Jokat et al., 1992). The coherent seismostratigraphy crossing these sites and correlations made between petrophysical properties measured on recovered sediments allowed construction of a single composite section that is described using four lithologic units (see the “[Expedition 302 summary](#)” chapter). The lithology of recovered sediments ranges from pyrite- and gypsum-enriched biosiliceous clays and oozes in the Paleogene to fossil-poor glaciomarine sediments in the Neogene (Figs. [F2](#), [F3](#)).

The composite sedimentary column from ACEX was generated from overlapping recovery in the upper ~30 meters below seafloor

<sup>1</sup>O'Regan, M., 2007. Data report: high-resolution bulk density, dry density, and porosity records from the Arctic Coring Expedition, IODP Expedition 302. In Backman, J., Moran, K., McInroy, D.B., Mayer, L.A., and the Expedition 302 Scientists, *Proc. IODP*, 302: Edinburgh (Integrated Ocean Drilling Program Management International, Inc.).

doi:10.2204/iodp.proc.302.201.2007

<sup>2</sup>Graduate School of Oceanography, University of Rhode Island, Narragansett RI 02882, USA.  
[oregan@gso.uri.edu](mailto:oregan@gso.uri.edu)



(mbsf) from Holes M0002A, M0004A, M0003A, and M0004C (Fig. F2). The remainder of the composite section is composed of material from two nonoverlapping holes: M0002A and M0004A. In the ideal situation, duplicate or triplicate recovery at a single drilling site (from two to three holes) provides substantial overlap. In the construction of a composite section, the overlapping recovery not only ensures that there are no stratigraphic gaps but also allows for careful selection and inclusion of the highest quality cored intervals. The limited overlap between the ACEX sites prevented exclusion of disturbed sections from the composite section. Although major coring disturbances were systematically described and tabulated (see Table T24 in the “Sites M0001–M0004” chapter), more common coring disturbances, such as compression or stretching of material during piston coring (APC) or undercutting during extended core barrel (XCB) operations are not recorded. These less dramatic disturbances can equally affect the quality of multisensor core logger (MSCL) measurements, as calibration algorithms used to calculate bulk density ( $\rho_B$ ) and compressional wave ( $P$ -wave) velocity require an accurate measurement of core diameter. Whole-core MSCL measurements, such as those performed during ACEX, are based on the diameter of the core liner but not the actual core.

Routine measurement of index properties on discrete samples during Ocean Drilling Program (ODP) and Integrated Ocean Drilling Program (IODP) expeditions provides a means for assessing the quality of MSCL data. Index properties, which include bulk density, grain density, dry density, and porosity, are termed moisture and density (MAD) measurements. They are determined by applying basic phase relationships to measurements of mass and volume (Blum, 1997). Although collected at a much lower resolution (one sample per section versus one sample every 1–2 cm), MAD measurements provide a more accurate and precise measurement of  $\rho_B$  than the MSCL estimate, which is derived from empirical relationships between gamma ray attenuation and the bulk density of aluminum/water mixtures (Blum, 1997; Boyce, 1976). Comparison between MAD- and MSCL-derived  $\rho_B$  at equivalent core positions (depths) can provide a means for both assessing and improving the quality of the MSCL data.

Here MAD data are used to correct  $\rho_B$  records from the MSCL. Using basic phase relationships, the corrected  $\rho_B$  logs, and the average grain density ( $\rho_G$ ) from the corresponding lithologic unit/subunit, high-resolution  $\rho_D$  and porosity ( $\phi$ ) records are generated. High-resolution  $\rho_D$  and  $\phi$  are useful data sets for calculating mass accumulation rates and investigat-

ing compaction processes at the ACEX drill sites on the Lomonosov Ridge.

## Methods

### Bulk density corrections

Bulk density is defined as the mass of a sample divided by the volume of the sample:

$$\rho_B = (\text{mass}/\text{volume}) =$$

$$[(m_{\text{solids}} + m_{\text{liquids}} + m_{\text{air}})/(v_{\text{solids}} + v_{\text{liquids}} + v_{\text{air}})]. \quad (1)$$

During ACEX, mass and volume were measured on subsamples from the recovered core and used for direct determinations of  $\rho_B$ . At sea, these MAD measurements were made on samples from core catchers (one per core) and performed on subsamples from split cores during the onshore phase of ACEX (~1 per section) (see the “[Sites M0001–M0004](#)” chapter). In the correction procedure outlined here, only shore-based measurements on split-cores are used. In addition to direct determinations of bulk density, MAD samples provide measurements of grain density ( $\rho_G$ ), dry density ( $\rho_D$ ), and porosity ( $\phi$ ) (see the “[Sites M0001–M0004](#)” chapter). These index properties are defined as

$$\rho_G = (m_{\text{solids}}/v_{\text{solids}}), \quad (2)$$

$$\rho_D = (m_{\text{solids}}/v_{\text{total}}), \text{ and} \quad (3)$$

$$\phi = (v_{\text{pore-water}}/v_{\text{total}}). \quad (4)$$

The MSCL also provides an estimate of sediment  $\rho_B$  and during ACEX was run at a sampling resolution of 2 cm on all visibly intact cores (see the “[Sites M0001–M0004](#)” chapter). The advantage of the MSCL is that it provides quick, nondestructive, high-resolution measurements. However, MSCL  $\rho_B$  is not a direct measurement and is derived from empirical relationships. The MSCL uses a  $^{137}\text{Cs}$  source to pass gamma rays through the core. Bulk density is estimated by measuring the attenuation of gamma rays (primarily through Compton scattering). The degree of attenuation is proportional to density and is dependent on the Compton mass absorption coefficient of the sample. Calibration of the system uses known seawater/aluminum standards and assumes that the attenuation coefficient of the sediments is proportional to that of aluminum. This assumption is largely valid for most siliciclastic sediments (Blum, 1997; Boyce, 1976). Hence, the quality of MSCL data is a function of core quality, the accuracy of the calibration, and the similarity of the Compton mass absorption coefficient of the sample to that of aluminum. Variations in any of these parameters can introduce errors into MSCL-derived  $\rho_B$ . To account for this variability, MAD  $\rho_B$  is used to derive a correc-



tion factor for MSCL  $\rho_B$ . Correction factors are determined separately for each core, accounting for inter-core variability in the quality of MSCL data.

MAD data from onshore analyses, where a Quantachrome pentapycnometer (helium-displacement pycnometer) was used to determine the volume of the subsamples, are compared to MSCL bulk density data from equivalent depths in each core.

Only samples that have a corresponding MSCL measurement from within 2 cm are used for determining the correction factors ( $cf$ ) defined as:

$$cf = \rho_{B-MSCL}/\rho_{B-MAD}. \quad (5)$$

Where more than a single MAD measurement exists for any core, the average correction factor for that core is calculated. If only a single MAD measurement was available, then the average correction factor for the lithologic unit/subunit is applied. This approach recognizes lithology-dependent variability in both core quality and Compton mass attenuation coefficients. MAD measurements and equivalent MSCL  $\rho_B$  data are given in Table T1. Correction factors for each core are listed in Table T2, and the average correction factor and grain density for lithologic units/subunits are shown in Table T3.

## Dry density and porosity

Similar to MAD data, where mass and volume measurements are used to calculate  $\phi$  and  $\rho_D$ , basic phase relationships can be used to derive these variables from the corrected high-resolution MSCL  $\rho_B$  records. The phase relationships require that  $\rho_G$  is known. For siliciclastic sediments a  $\rho_G$  of 2.70–2.75 g/cm<sup>3</sup> is often assumed. Instead of assuming the  $\rho_G$ , the average value is taken from MAD measurements in the corresponding lithologic unit/subunit (Table T3). More variable grain densities in lithologic Units 1.6 and 3 are attributed to the widespread occurrence of authigenic minerals such as pyrite (see the “[Sites M0001–M0004](#)” chapter; Stein et al., 2006). For lithologic Unit 3, a relatively high standard deviation is observed for the average grain density ( $\rho_G = 2.54 \pm 0.14$  g/cm<sup>3</sup>), which can be reduced by subdividing the unit into petrophysical Subunits 3a and 3b. The subdivision is placed between Cores 302-M0004A-23X and 27X and results in a mean  $\rho_G$  for petrophysical Subunit 3a of  $2.43 \pm 0.06$  g/cm<sup>3</sup> and for Subunit 3b of  $2.67 \pm 0.08$  g/cm<sup>3</sup> (Table T3; Fig. F5). This break occurs during a prolonged interval of no recovery (Fig. F2), preventing an exact depth to be associated with the division or determination of whether the break is abrupt or gradual.

Porosity and dry density are determined from the corrected  $\rho_B$  using the phase relationships:

$$\phi = (\rho_G - \rho_B)/(\rho_G - \rho_F), \text{ and} \quad (6)$$

$$\rho_D = [(\rho_B - \rho_F)/(\rho_G - 1)]\rho_G, \quad (7)$$

where  $\rho_G$  is the average grain density from the corresponding lithologic unit/subunit (g/cm<sup>3</sup>),  $\rho_B$  is the corrected MSCL bulk density (g/cm<sup>3</sup>),  $\rho_D$  is the dry density (g/cm<sup>3</sup>),  $\phi$  is the porosity (unitless), and  $\rho_F$  is an assumed pore fluid density of 1.024 g/cm<sup>3</sup>.

## Results and discussion

The quality of the dry density and porosity logs generated from the high-resolution MSCL data is dependent on the quality of the MSCL bulk density data. Despite the high linear correlation coefficient between the MAD and uncorrected MSCL  $\rho_B$ , MSCL-derived values are generally higher than depth-equivalent MAD measurements. The overprediction is greater at higher sediment  $\rho_B$  (Fig. F4). The correction procedure developed here reduces both the overall offset and the scatter that arises from variability in the core quality (Fig. F4).

The complete downhole corrected MSCL  $\rho_B$  data set shows close agreement with the MAD data (Fig. F5). Similar agreement is seen in the derived  $\rho_D$  and  $\phi$  data. The only core that showed significant deviation between the corrected MSCL and the MAD  $\rho_B$  was 302-M0002A-23X. Here a single MAD measurement from Section 302-M0002A-23X-2 was used to develop the correction factor and provided a much better fit than the average correction factor from lithologic Subunit 1.3. Increased divergence between the MAD and MSCL predictions of  $\rho_D$  and  $\phi$  data is introduced by using the average grain density for lithologic units/subunits in Equations 6 and 7. This assumption overlooks any natural variability in sediment composition. Between Subunits 1.1 and 1.5, this natural variability would include proportional changes in the sand, silt, and clay contents of the sediments, as well as the presence of authigenic iron-manganese minerals (see the “[Sites M0001–M0004](#)” chapter) that characteristically have a higher  $\rho_G$  than generic silty clays.

Beneath Subunit 1.5, increased variability in the occurrence and quantity of total organic carbon and authigenic minerals such as pyrite (Stein et al., 2006) make the use of the average  $\rho_G$  more problematic. For instance, although quartz has a  $\rho_G$  of 2.65 g/cm<sup>3</sup>, pyrite has a grain density of 5.02 g/cm<sup>3</sup>, introducing large variability in the  $\rho_B$  logs from the MSCL. This

variability is not adequately sampled in the discrete MAD data nor is it accounted for by employing average  $\rho_G$ . Below Core 302-M0004A-28X (Fig. F2), there are no MAD measurements to correct the MSCL data. The average correction factors for lithologic Unit 3 and  $\rho_G$  from petrophysical Subunit 3b were used to correct the  $\rho_B$  and generate the  $\rho_D$  and  $\phi$  logs for these cores.

The  $\rho_B$ ,  $\rho_D$ , and  $\phi$  data from this study are available in Table T4. The MSCL data include measurements that were made on sediments described as disturbed in Table T24 in the “Sites M0001–M0004” chapter. How the results from this study are applied to future research depends on the nature and resolution of the work. To a first order, the use of average grain densities for lithologic units and subunits in Equations 6 and 7 introduces an error into the dry density and porosity data. This error may exaggerate absolute differences between units and subunits but does not diminish the significance of the variability within them. Through sections where sediments are believed to be relatively homogeneous, a depth-dependent relationship for dry density can be derived and used in mass accumulation rate calculations (e.g., see Moran, 1997). Filtering of the data to remove sections with known core disturbances is certainly recommended (e.g., see caption for Fig. F5). Once cleaned, artificial variability in the data can be reduced by applying a generous smoothing function, the size of which should depend on the resolution of the study.

## Conclusions

The corrected  $\rho_B$  and derived  $\rho_D$  and  $\phi$  logs from the MSCL data presented here provide improved and higher resolution petrophysical data sets for ongoing studies of the ACEX sediments. The  $\rho_D$  records are a necessary requirement for calculating mass accumulation rates, whereas the  $\phi$  data can be used to investigate compaction-related processes at the ACEX site and, through integration with seismic data, regional lithology-dependent trends. However, variability remains in these records that is not entirely associated with in situ lithologic change.

On future expeditions, improved MSCL data quality can be obtained with overlapping recovery from which high-quality cores can be selectively used in the construction of the composite section, higher

resolution MAD sampling for comparison and correction of the MSCL data, and finally, when possible, the use of split-core MSCL systems that remove uncertainties associated with variations in core thicknesses.

## Acknowledgments

Financial support was provided by the National Science Foundation (NSF) and the U.S. Science Support Program (USSP) of Joint Oceanographic Institutions (JOI), Inc. This research was conducted with samples and data from the Integrated Ocean Drilling Program (IODP), an international marine research program dedicated to advancing scientific understanding of the Earth, the deep biosphere, climate change, and Earth processes by sampling and monitoring subseafloor environments.

## References

- Blum, P., 1997. Physical properties handbook: a guide to the shipboard measurement of physical properties of deep-sea cores. *ODP Tech. Note*, 26. doi:[10.2973/odp.tn.26.1997](https://doi.org/10.2973/odp.tn.26.1997)
- Boyce, R.E., 1976. Definitions and laboratory techniques of compressional sound velocity parameters and wet-water content, wet-bulk density, and porosity parameters by gravimetric and gamma-ray attenuation techniques. In Schlanger, S.O., Jackson, E.D., et al., *Init. Repts. DSDP*, 33: Washington, DC (U.S. Govt. Printing Office), 931–958. doi:[10.2973/dsdp.proc.33.1976](https://doi.org/10.2973/dsdp.proc.33.1976)
- Moran, K., 1997. Elastic property corrections applied to Leg 154 sediment, Ceara Rise. In Shackleton, N.J., Curry, W.B., Richter, C., and Bralower, T.J. (Eds.), *Proc. ODP, Sci. Results*, 154: College Station, TX (Ocean Drilling Program), 151–155. doi:[10.2973/odp.proc.sr.154.132.1997](https://doi.org/10.2973/odp.proc.sr.154.132.1997)
- Jokat, W., Uenzelmann-Neben, G., Kristoffersen, Y., and Rasmussen, T.M., 1992. Lomonosov Ridge—a double-sided continental margin. *Geology*, 20(10):887–890. doi:[10.1130/0091-7613\(1992\)020<0887:LRADSC>2.3.CO;2](https://doi.org/10.1130/0091-7613(1992)020<0887:LRADSC>2.3.CO;2)
- Stein, R., Boucsein, B., and Meyer, H., 2006. Anoxia and high primary production in the Paleogene central Arctic Ocean: first detailed records from Lomonosov Ridge. *Geophys. Res. Lett.*, 33:L18606. doi:[10.1029/2006GL026776](https://doi.org/10.1029/2006GL026776)

**Initial receipt:** 30 May 2007

**Acceptance:** 22 October 2007

**Publication:** 17 January 2007

**MS 302-201**



**Figure F1.** Location map and seismic profile AWI-91090 showing positions of sites visited during Expedition 302. ACEX = Arctic Coring Expedition.

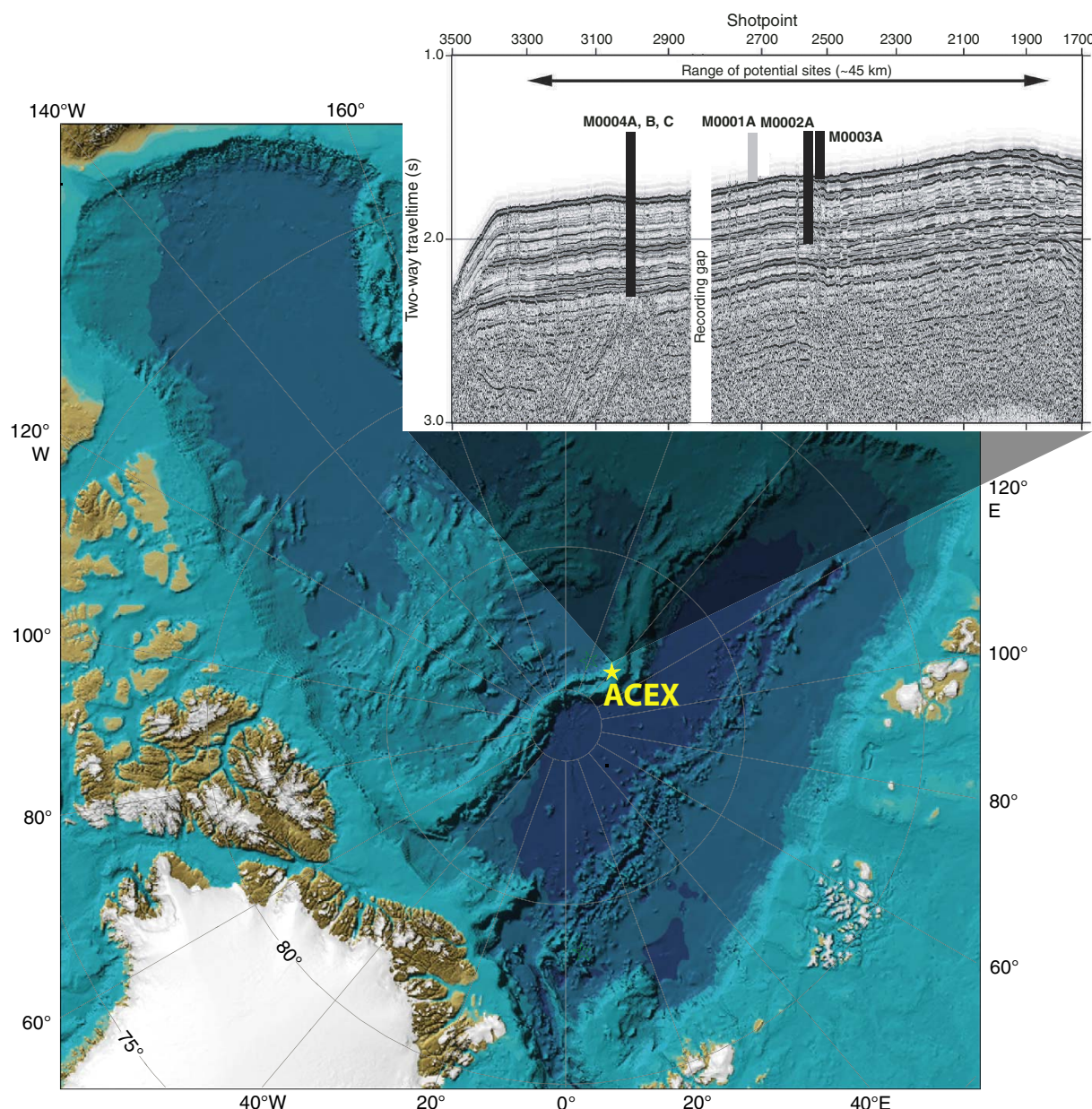


**Figure F2.** Core recovery diagram for all Expedition 302 holes. Black = recovered core, white = no core recovery, shaded = washed intervals (from the “[Sites M0001–M0004](#)” chapter).

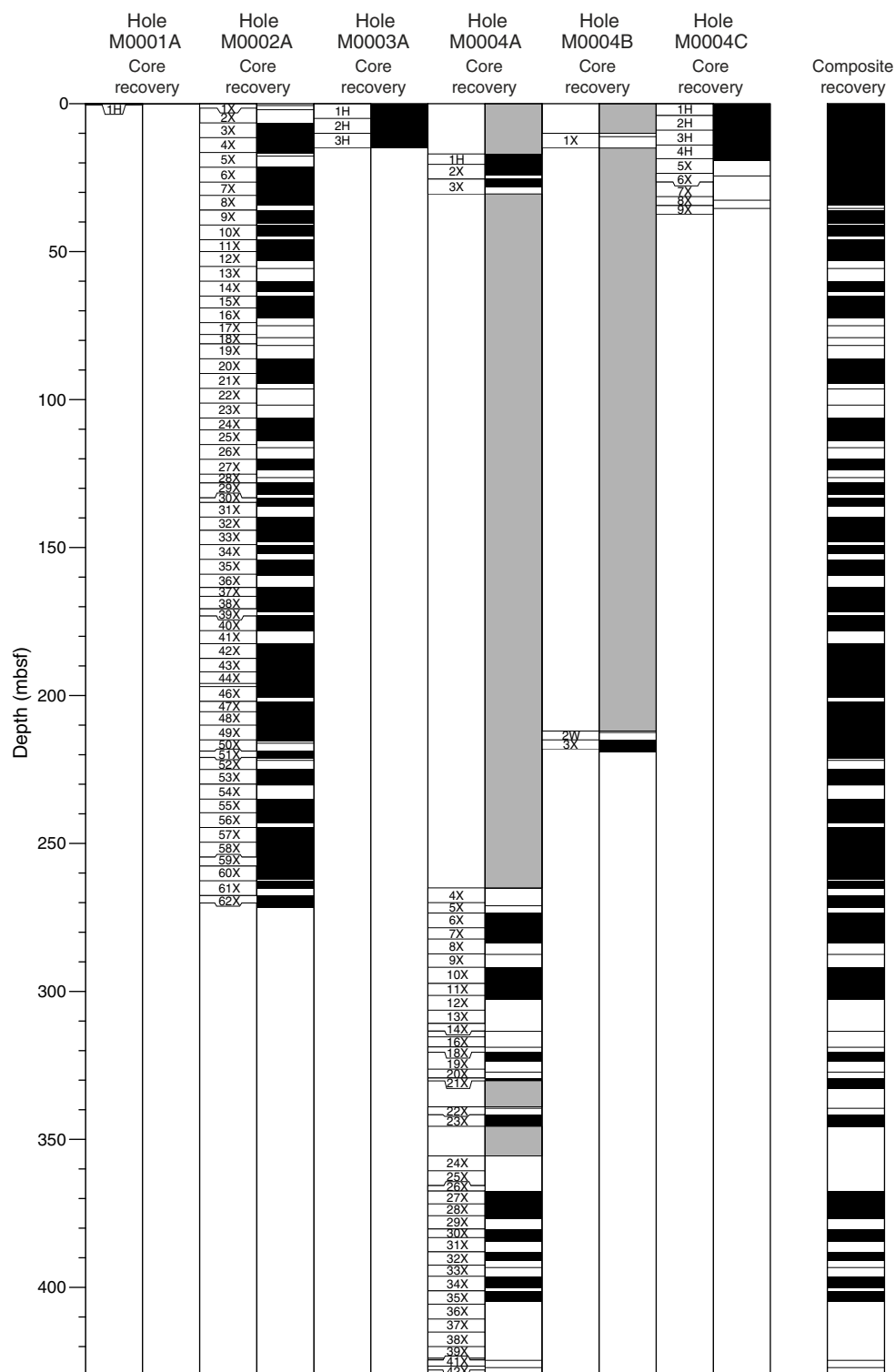


**Figure F3.** Lithostratigraphic column with age estimates and unit/subunit descriptions of sediments recovered during Expedition 302. XRD = X-ray diffraction (adapted from the “[Sites M0001–M0004](#)” chapter).

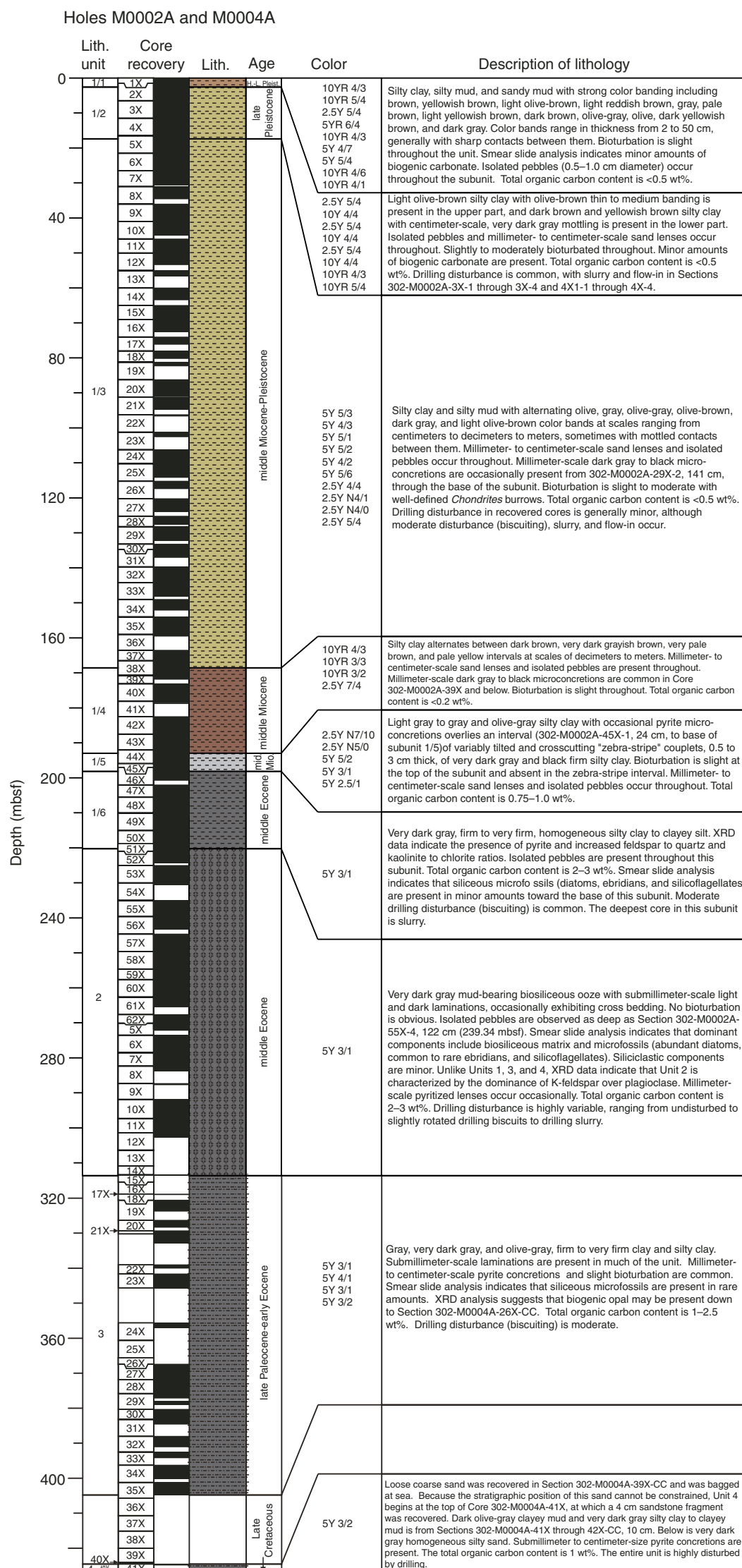


**Figure F4.** Crossplots of MSCL and MAD  $\rho_B$  and  $\rho_D$ . A. Corrected and uncorrected MSCL  $\rho_B$  at equivalent depths to MAD  $\rho_B$  measurements. B. Corrected and MSCL  $\rho_B$  at equivalent depths to MAD  $\rho_B$  measurements with lithologic units/subunits color-coded. C. Corrected MSCL-derived  $\rho_D$  at equivalent depths to MAD  $\rho_D$  measurements with lithologic units/subunits color-coded.

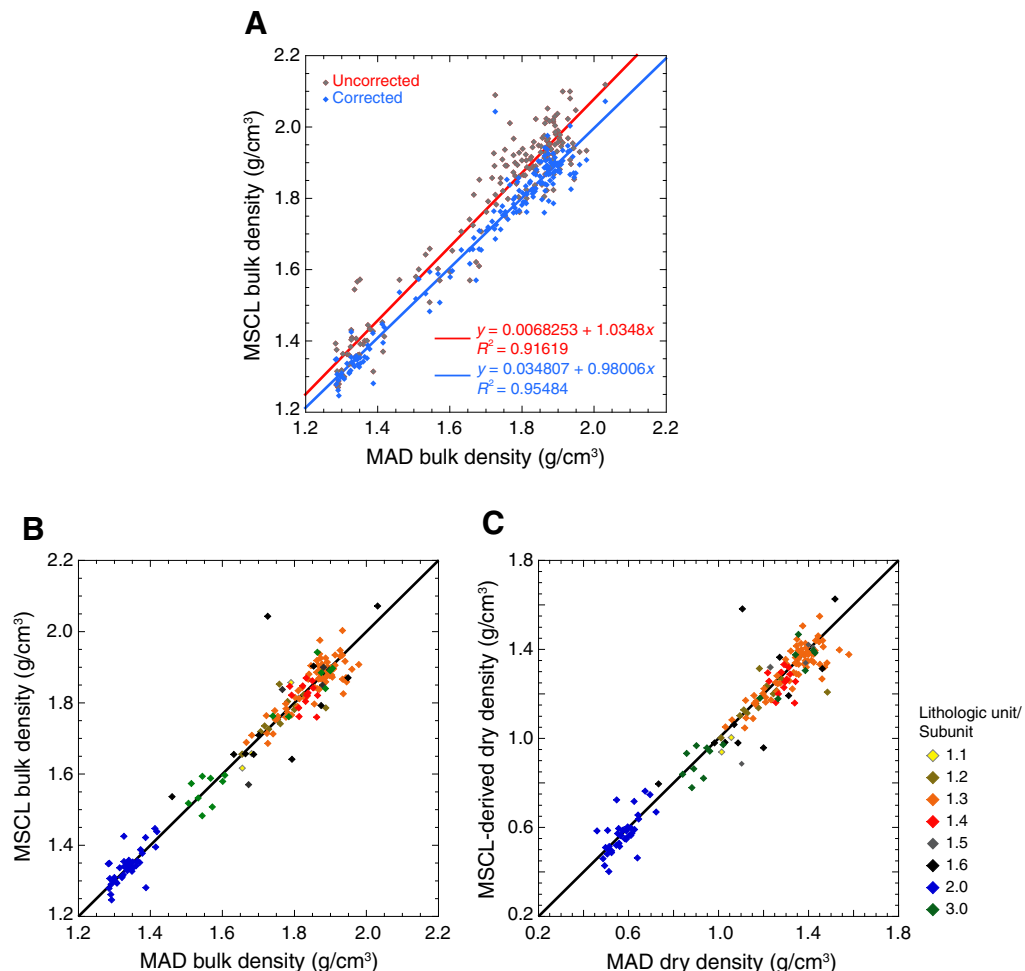


**Figure F5.** Downhole corrected and derived MSCL data and MAD measurements of  $\rho_B$ ,  $\rho_D$ , and  $\phi$ . Data have been cleaned by removing all  $\rho_B$  measurements  $<1.2 \text{ g/cm}^3$ , the top 5 cm from all sections, the last measurement from all sections, and all data corresponding to disturbed intervals as tabulated in T24 from the “Sites M0001–M0004” chapter. Average grain density for lithologic unit/subunits are used to calculate  $\rho_D$  and  $\phi$  from corrected MSCL  $\rho_B$  and are shown on  $\rho_D$  downhole plots. Data have not been migrated onto composite depth scale. Colors indicate hole from which MAD data is taken (red = Hole M0004C, blue = Hole M0002A, green = Hole M0004A).

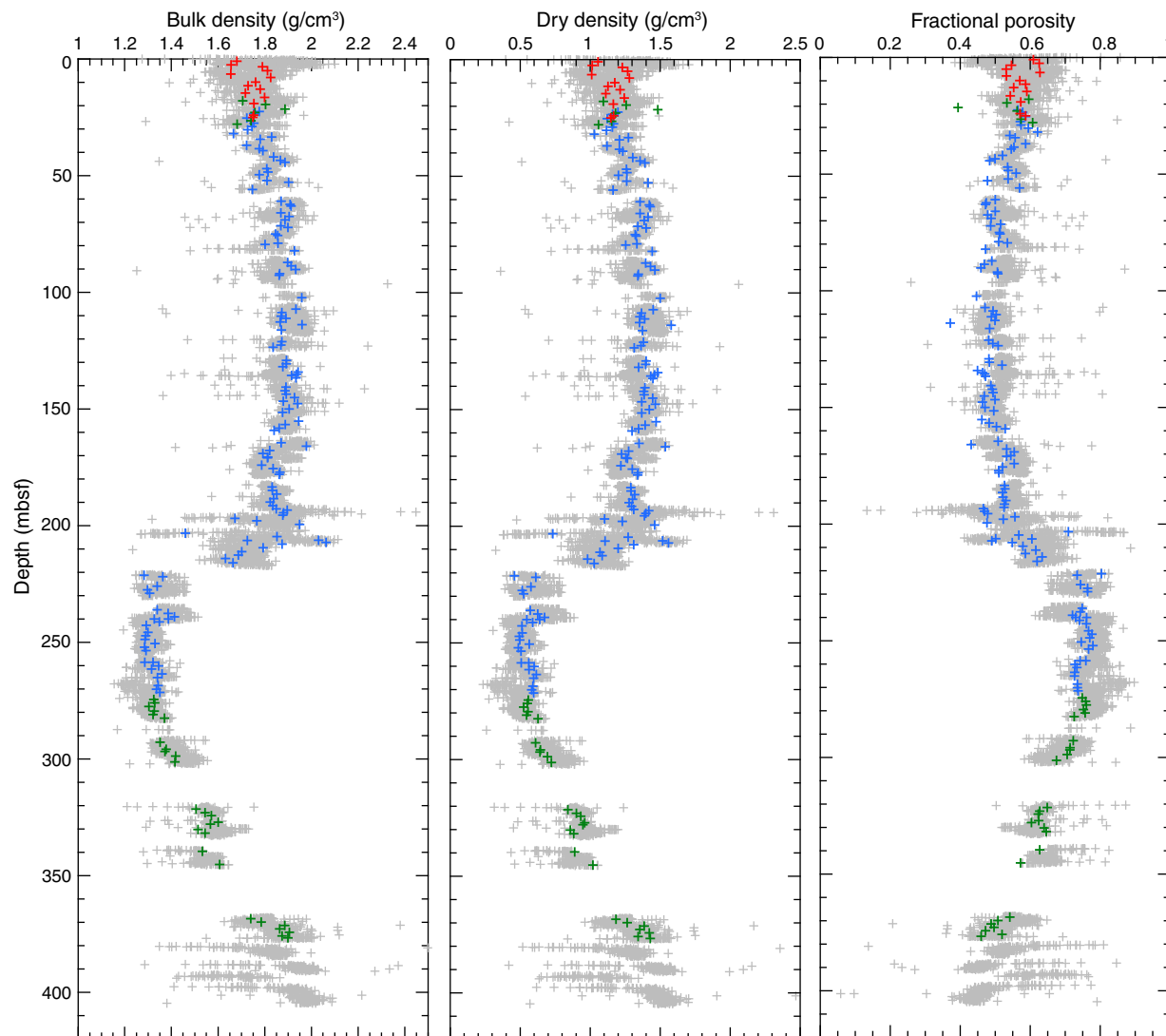


**Table T1.** MAD data and equivalent MSCL  $\rho_B$  data used to derive correction factors. (See table notes. Continued on next two pages.)

Core, section, interval (cm)	Depth (mbsf)	Water content (%)		Density (g/cm <sup>3</sup> )			Porosity (%)	Void ratio	MSCL density (g/cm <sup>3</sup> )	Depth difference (m)	MSCL/MAD bulk density	
		Wet	Dry	Bulk	Dry	Grain					Discrete	Core average
<b>302-M0002A-</b>												
6X-1, 100–102	22.50	32.57	48.30	1.78	1.20	2.76	56.52	1.30	1.97	0.00	1.107	1.103
6X-2, 166–68	23.53	33.82	51.10	1.75	1.16	2.75	57.88	1.37	1.94	0.01	1.105	
6X-3, 100–102	25.37	34.88	53.57	1.72	1.12	2.72	58.72	1.42	1.89	0.01	1.097	
7X-1, 100–102	27.50	33.40	50.15	1.75	1.17	2.73	57.21	1.34	1.89	0.00	1.079	1.074
7X-2, 100–102	29.00	33.66	50.74	1.75	1.16	2.72	57.38	1.35	1.91	0.00	1.094	
7X-3, 89–91	30.39	35.30	54.56	1.73	1.12	2.76	59.50	1.47	1.81	0.01	1.049	
8X-1, 100–102	32.00	38.15	61.68	1.67	1.03	2.72	62.09	1.64	1.81	0.00	1.086	1.072
8X-2, 100–102	33.50	30.36	43.59	1.83	1.27	2.78	54.23	1.18	1.94	0.00	1.062	
8X-3, 85–87	34.45	32.05	47.17	1.78	1.21	2.73	55.73	1.26	1.90	0.01	1.067	
9X-1, 100–102	37.00	34.93	53.68	1.72	1.12	2.72	58.73	1.42	1.93	0.00	1.119	1.092
9X-2, 100–102	38.50	31.91	46.86	1.78	1.21	2.71	55.35	1.24	1.92	0.00	1.081	
9X-3, 30–32	39.30	31.19	45.34	1.79	1.23	2.72	54.60	1.20	1.93	0.00	1.076	
10X-2, 100–102	43.50	27.39	37.72	1.87	1.36	2.71	49.95	1.00	2.02	0.00	1.083	1.084
10X-1, 100–102	42.00	29.04	40.93	1.84	1.30	2.73	52.13	1.09	2.02	0.00	1.100	
10X-3, 30–32	44.30	26.30	35.68	1.89	1.39	2.70	48.46	0.94	2.01	0.00	1.068	
11X-1, 100–102	47.00	30.33	43.52	1.81	1.26	2.71	53.57	1.15	1.86	0.00	1.031	1.042
11X-2, 100–102	48.49	30.34	43.56	1.81	1.26	2.73	53.75	1.16	1.89	0.01	1.041	
11X-3, 60–62	49.60	32.30	47.71	1.78	1.20	2.73	56.03	1.27	1.87	0.00	1.054	
12X-2, 60–62	52.12	30.37	43.61	1.81	1.26	2.72	53.69	1.16	1.92	0.00	1.062	1.048
12X-3, 30–32	52.82	25.73	34.64	1.90	1.41	2.71	47.81	0.92	1.97	0.00	1.035	
13X-1, 100–102	56.00	33.39	50.14	1.75	1.16	2.70	56.98	1.32	1.82	0.00	1.042	NA
14X-1, 100–102	61.00	27.41	37.76	1.87	1.36	2.72	50.06	1.00	1.94	0.00	1.038	1.027
14X-2, 80–82	62.31	25.46	34.16	1.91	1.42	2.71	47.45	0.90	1.95	0.01	1.019	
14X-3, 60–62	63.11	25.28	33.83	1.91	1.43	2.71	47.22	0.89	1.96	0.01	1.023	
15X-1, 100–102	66.00	27.43	37.80	1.87	1.36	2.72	50.06	1.00	1.82	0.00	0.975	0.992
15X-2, 100–102	67.51	25.75	34.69	1.90	1.41	2.71	47.91	0.92	1.88	0.01	0.988	
15X-3, 100–102	69.00	26.52	36.09	1.89	1.39	2.71	48.86	0.96	1.91	0.00	1.012	
16X-2, 100–102	71.50	28.25	39.37	1.87	1.34	2.77	51.56	1.06	1.96	0.00	1.049	1.048
16X-3, 20–23	72.21	26.26	35.61	1.90	1.40	2.73	48.71	0.95	1.99	0.01	1.048	
17X-1, 100–102	75.00	28.42	39.71	1.85	1.32	2.71	51.24	1.05	1.95	0.00	1.055	1.023
17X-2, 20–22	75.71	28.39	39.64	1.86	1.33	2.74	51.44	1.06	1.84	0.01	0.991	
18X-1, 100–102	79.00	28.15	39.18	1.86	1.33	2.72	51.04	1.04	1.97	0.00	1.061	1.068
18X-2, 10–12	79.55	30.39	43.66	1.80	1.25	2.70	53.48	1.15	1.94	0.01	1.076	
19X-1, 100–102	82.20	25.12	33.54	1.93	1.44	2.74	47.27	0.90	2.02	0.00	1.050	NA
20X-1, 100–102	87.20	26.46	35.98	1.90	1.40	2.74	49.06	0.96	2.04	0.00	1.073	1.086
20X-2, 100–102	88.71	25.13	33.56	1.91	1.43	2.70	46.94	0.88	2.10	0.01	1.098	
20X-3, 100–102	90.21	24.32	32.14	1.93	1.46	2.71	45.92	0.85	2.10	0.01	1.086	
21X-1, 80–82	92.00	27.82	38.53	1.86	1.35	2.73	50.63	1.03	1.93	0.00	1.034	1.047
21X-2, 100–102	92.71	27.93	38.75	1.86	1.34	2.73	50.79	1.03	1.98	0.01	1.061	
23X-2, 100–102	102.33	23.37	30.50	1.96	1.50	2.71	44.71	0.81	1.94	0.01	0.992	NA
24X-1, 100–102	107.20	24.97	33.27	1.93	1.45	2.74	47.14	0.89	1.91	0.00	0.986	1.022
24X-2, 100–102	108.69	27.03	37.04	1.87	1.37	2.70	49.44	0.98	1.97	0.01	1.051	
24X-3, 110–112	110.30	27.55	38.03	1.87	1.35	2.73	50.32	1.01	1.92	0.00	1.028	
25X-1, 100–102	111.20	26.48	36.02	1.89	1.39	2.72	48.91	0.96	1.95	0.00	1.031	1.019
25X-2, 100–102	112.71	27.43	37.80	1.87	1.35	2.71	49.98	1.00	1.94	0.01	1.041	
25X-3, 70–72	113.92	19.41	24.09	1.96	1.58	2.51	37.16	0.59	1.93	0.00	0.985	
26X-1, 100–102	116.20	26.51	36.08	1.87	1.37	2.67	48.44	0.94	2.05	0.00	1.097	NA
27X-1, 100–102	121.20	26.32	35.72	1.87	1.38	2.66	48.16	0.93	1.89	0.00	1.006	1.010
27X-2, 100–102	122.70	27.03	37.04	1.87	1.36	2.69	49.34	0.97	1.91	0.00	1.022	
27X-3, 40–42	123.61	28.36	39.58	1.84	1.32	2.68	50.84	1.03	1.84	0.01	1.000	
29X-1, 100–102	129.20	26.09	35.31	1.89	1.40	2.70	48.25	0.93	1.98	0.00	1.045	1.045
29X-2, 100–102	130.70	26.18	35.47	1.89	1.40	2.71	48.39	0.94	1.99	0.00	1.049	
29X-3, 70–72	131.90	28.34	39.54	1.88	1.35	2.80	51.97	1.08	1.95	0.00	1.040	
30X-1, 100–102	134.20	23.69	31.04	1.94	1.48	2.69	44.95	0.82	1.94	0.00	0.999	1.000
30X-2, 100–102	135.71	25.15	33.59	1.92	1.43	2.71	47.03	0.89	1.93	0.01	1.008	
30X-3, 50–52	136.71	25.02	33.37	1.93	1.45	2.75	47.25	0.90	1.92	-0.01	0.992	
31X-1, 50–52	135.20	24.55	32.55	1.94	1.46	2.73	46.42	0.87	1.90	0.00	0.979	NA
32X-1, 100–102	140.70	26.42	35.90	1.89	1.39	2.72	48.78	0.95	2.03	0.00	1.073	1.068
32X-2, 100–102	142.20	26.69	36.40	1.89	1.38	2.72	49.17	0.97	2.02	0.00	1.071	
32X-3, 100–102	143.71	26.75	36.52	1.89	1.39	2.74	49.41	0.98	2.00	0.01	1.059	
33X-1, 100–102	145.20	24.92	33.19	1.93	1.45	2.73	46.90	0.88	1.97	0.00	1.021	1.020
33X-2, 100–102	146.71	27.21	37.39	1.88	1.37	2.73	49.96	1.00	1.94	0.01	1.031	



Table T1 (continued).

Core, section, interval (cm)	Depth (mbsf)	Water content (%)		Density (g/cm <sup>3</sup> )			Porosity (%)	Void ratio	MSCL density (g/cm <sup>3</sup> )	Depth difference (m)	MSCL/MAD bulk density	
		Wet	Dry	Bulk	Dry	Grain					Discrete	Core average
33X-3, 50–52	147.73	24.47	32.40	1.94	1.47	2.73	46.38	0.87	1.95	0.01	1.007	
34X-1, 100–102	150.00	25.31	33.89	1.91	1.42	2.69	47.09	0.89	1.98	0.00	1.038	1.056
34X-2, 100–102	151.50	27.07	37.13	1.88	1.37	2.72	49.61	0.98	2.02	0.00	1.075	
35X-2, 97–99	155.24	24.32	32.14	1.94	1.47	2.74	46.19	0.86	1.85	0.00	0.953	0.997
35X-3, 100–102	156.76	26.18	35.46	1.89	1.39	2.69	48.27	0.93	1.87	0.00	0.989	
35X-4, 100–102	158.27	27.71	38.33	1.86	1.35	2.71	50.40	1.02	1.91	0.01	1.027	
35X-5, 40–42	159.19	29.42	41.68	1.84	1.30	2.76	52.87	1.12	1.88	0.01	1.019	
37X-1, 100–102	164.50	27.85	38.60	1.87	1.35	2.75	50.87	1.04	1.96	0.00	1.050	1.014
37X-2, 100–102	166.01	22.32	28.74	1.98	1.54	2.70	43.14	0.76	1.93	0.01	0.977	
38X-2, 100–102	167.89	29.95	42.75	1.82	1.28	2.73	53.27	1.14	1.88	0.01	1.034	1.022
38X-3, 100–102	169.08	31.67	46.35	1.79	1.22	2.75	55.42	1.24	1.86	0.00	1.039	
38X-4, 110–112	170.69	30.76	44.43	1.81	1.26	2.76	54.46	1.20	1.80	0.01	0.993	
39X-1, 30–32	170.98	30.13	43.12	1.81	1.27	2.71	53.31	1.14	1.82	0.00	1.007	NA
40X-1, 100–102	174.08	31.78	46.59	1.79	1.22	2.74	55.47	1.25	1.89	0.00	1.059	1.013
40X-2, 100–102	175.58	29.08	40.99	1.84	1.30	2.72	52.12	1.09	1.87	0.00	1.020	
40X-3, 100–102	177.09	28.01	38.92	1.86	1.34	2.74	51.01	1.04	1.87	0.01	1.002	
40X-4, 50–52	178.09	28.10	39.08	1.86	1.34	2.74	51.10	1.04	1.81	0.01	0.969	
42X-1, 100–102	183.49	29.47	41.78	1.83	1.29	2.73	52.70	1.11	1.89	0.00	1.032	1.047
42X-2, 100–102	184.99	29.52	41.88	1.83	1.29	2.74	52.83	1.12	1.96	0.00	1.069	
42X-3, 100–102	186.49	28.82	40.50	1.85	1.32	2.75	52.13	1.09	1.93	0.00	1.042	
43X-1, 100–102	188.49	29.10	41.04	1.84	1.30	2.73	52.23	1.09	1.89	0.00	1.028	1.034
43X-2, 100–102	189.98	29.82	42.50	1.82	1.28	2.73	53.10	1.13	1.91	0.01	1.048	
43X-3, 100–102	191.49	29.39	41.63	1.83	1.30	2.74	52.67	1.11	1.88	0.00	1.026	
44X-1, 84–86	192.83	29.10	41.05	1.85	1.31	2.76	52.57	1.11	1.90	0.00	1.027	
44X-1, 14–146	193.43	25.16	33.61	1.90	1.42	2.66	46.60	0.87	1.93	0.00	1.018	
44X-2, 100–102	194.49	25.60	34.40	1.88	1.40	2.64	47.01	0.89	1.94	0.00	1.031	1.020
44X-3, 60–62	195.60	26.12	35.36	1.88	1.39	2.66	47.91	0.92	1.89	0.01	1.005	
45X-1, 100–102	196.93	34.06	51.66	1.67	1.10	2.49	55.64	1.25	1.62	0.00	0.969	NA
46X-1, 100–102	198.00	30.34	43.56	1.77	1.23	2.58	52.33	1.10	2.01	0.00	1.138	1.094
46X-2, 100–102	199.50	25.04	33.41	1.95	1.46	2.79	47.66	0.91	2.05	0.00	1.050	
47X-2, 100–102	203.26	49.76	99.06	1.46	0.73	2.53	70.97	2.44	1.57	0.00	1.076	1.023
47X-3, 100–102	204.76	31.37	45.71	1.85	1.27	2.94	56.77	1.31	1.95	0.00	1.050	
47X-4, 100–102	206.27	25.29	33.84	2.03	1.52	3.04	50.15	1.01	2.12	0.01	1.043	
47X-5, 40–42	207.19	24.36	32.20	2.06	1.56	3.06	49.06	0.96	1.90	0.01	0.921	
48X-1, 90–92	206.40	35.90	56.00	1.73	1.11	2.80	60.50	1.53	2.09	0.00	1.211	1.004
48X-2, 100–102	208.00	30.00	42.85	1.87	1.31	2.91	54.90	1.22	1.92	0.00	1.026	
48X-2, 100–102	209.51	33.08	49.42	1.79	1.20	2.85	57.92	1.38	1.76	0.01	0.982	
49X-2, 100–102	211.15	37.12	59.03	1.70	1.07	2.79	61.66	1.61	1.76	0.00	1.036	1.031
49X-3, 100–102	212.65	35.59	55.27	1.69	1.09	2.63	58.64	1.42	1.71	0.00	1.012	
49X-4, 100–102	214.16	39.80	66.10	1.63	0.98	2.68	63.41	1.73	1.71	0.01	1.046	
50X-1, 100–102	216.00	38.16	61.71	1.66	1.03	2.71	62.01	1.63	1.72	0.00	1.036	NA
51X-2, 102–104	221.27	64.15	178.93	1.28	0.46	2.34	80.38	4.10	1.39	0.01	1.086	NA
52X-1, 102–104	221.96	55.14	122.91	1.36	0.61	2.30	73.42	2.76	1.40	0.00	1.027	NA
53X-1, 102–104	226.02	56.91	132.08	1.34	0.58	2.25	74.41	2.91	1.36	0.00	1.013	1.004
53X-2, 102–104	227.54	60.33	152.06	1.30	0.51	2.19	76.44	3.25	1.31	0.00	1.006	
53X-3, 102–104	229.04	59.86	149.10	1.31	0.52	2.23	76.42	3.24	1.30	0.00	0.994	
55X-2, 102–104	236.12	57.24	133.87	1.34	0.57	2.28	74.88	2.98	1.35	0.00	1.011	1.004
55X-3, 102–104	237.63	54.90	121.74	1.39	0.63	2.44	74.33	2.90	1.43	0.01	1.029	
55X-4, 102–104	239.14	52.28	109.57	1.41	0.67	2.42	72.14	2.59	1.45	0.00	1.028	
55X-5, 42–44	240.05	53.88	116.82	1.39	0.64	2.37	73.00	2.70	1.31	0.01	0.947	
56X-1, 42–44	240.02	58.75	142.44	1.33	0.55	2.29	76.12	3.19	1.43	0.00	1.078	1.026
56X-2, 102–104	241.25	56.26	128.64	1.35	0.59	2.28	74.10	2.86	1.36	0.01	1.010	
56X-3, 102–104	242.76	60.31	151.98	1.29	0.51	2.15	76.10	3.18	1.28	0.00	0.990	
57X-2, 102–104	245.75	60.43	152.73	1.30	0.51	2.21	76.70	3.29	1.32	0.01	1.014	1.006
57X-3, 102–104	247.25	61.68	160.95	1.29	0.49	2.22	77.71	3.49	1.27	0.01	0.984	
57X-4, 102–104	248.76	61.30	158.42	1.29	0.50	2.17	77.07	3.36	1.32	0.00	1.021	
58X-1, 102–104	250.62	57.47	135.10	1.33	0.57	2.23	74.64	2.94	1.33	0.00	1.003	0.998
58X-2, 102–104	252.12	62.13	164.04	1.29	0.49	2.21	77.98	3.54	1.28	0.00	0.993	
58X-3, 102–104	253.63	60.82	155.23	1.29	0.51	2.17	76.68	3.29	1.29	0.01	0.997	
59X-3, 102–104	258.63	60.50	153.16	1.29	0.51	2.11	75.96	3.16	1.38	0.01	1.070	NA
60X-1, 100–102	258.60	57.54	135.52	1.32	0.56	2.18	74.24	2.88	1.33	0.00	1.010	1.019
60X-2, 100–102	260.11	55.43	124.36	1.34	0.60	2.20	72.80	2.68	1.36	0.01	1.011	
60X-3, 90–92	261.52	57.15	133.39	1.31	0.56	2.12	73.39	2.76	1.36	0.00	1.036	
61X-1, 100–102	263.60	54.77	121.10	1.36	0.62	2.26	72.75	2.67	1.39	0.00	1.022	1.036
61X-2, 100–102	265.11	55.51	124.79	1.34	0.60	2.18	72.65	2.66	1.41	0.01	1.050	
62X-1, 100–102	268.60	56.04	127.47	1.34	0.59	2.23	73.49	2.77	1.57	0.00	1.166	1.162
62X-2, 100–102	270.11	56.35	129.11	1.34	0.58	2.20	73.50	2.77	1.54	0.01	1.156	



Table T1 (continued).

Core, section, interval (cm)	Depth (mbsf)	Water content (%)		Density (g/cm <sup>3</sup> )			Porosity (%)	Void ratio	MSCL density (g/cm <sup>3</sup> )	Depth difference (m)	MSCL/MAD bulk density	
		Wet	Dry	Bulk	Dry	Grain					Discrete	Core average
62X-3, 90–92	271.51	55.88	126.68	1.35	0.60	2.27	73.72	2.81	1.57	0.01	1.164	
302-M0004A-												
1H-1, 100–102	18.00	35.80	55.76	1.71	1.10	2.71	59.64	1.48	1.79	0.00	1.050	1.042
1H-2, 100–102	19.51	30.30	43.47	1.80	1.26	2.70	53.37	1.14	1.87	0.01	1.034	
2X-1, 100–102	21.50	21.37	27.17	1.89	1.48	2.45	39.38	0.65	1.82	0.00	0.966	1.021
2X-2, 100–102	23.00	32.79	48.79	1.76	1.18	2.70	56.30	1.29	1.89	0.00	1.076	
3X-1, 102–104	26.52	33.76	50.96	1.74	1.15	2.71	57.39	1.35	1.86	0.00	1.066	1.084
3X-2, 102–104	28.02	36.98	58.67	1.68	1.06	2.70	60.72	1.55	1.85	0.00	1.101	
6X-1, 102–104	274.52	57.89	137.48	1.32	0.56	2.22	74.90	2.98	1.38	0.00	1.045	1.051
6X-2, 102–104	276.02	58.48	140.83	1.33	0.55	2.28	75.86	3.14	1.41	0.00	1.061	
6X-3, 102–104	277.53	59.74	148.39	1.30	0.52	2.19	76.05	3.17	1.36	0.01	1.046	
7X-1, 102–104	279.52	58.07	138.49	1.33	0.56	2.25	75.23	3.04	1.40	0.00	1.058	1.036
7X-2, 102–104	281.04	58.70	142.11	1.32	0.55	2.25	75.74	3.12	1.36	0.00	1.029	
7X-3, 102–104	282.55	54.25	118.57	1.37	0.63	2.29	72.60	2.65	1.40	0.01	1.022	
10X-1, 102–104	292.87	54.80	121.25	1.35	0.61	2.21	72.33	2.61	1.39	0.01	1.030	1.041
10X-2, 102–104	295.87	53.13	113.34	1.38	0.65	2.26	71.46	2.50	1.43	0.01	1.041	
10X-3, 40–42	296.78	53.23	113.83	1.37	0.64	2.24	71.37	2.49	1.44	0.00	1.052	
11X-2, 102–104	298.82	50.96	103.90	1.42	0.70	2.36	70.58	2.40	1.41	0.00	0.996	0.982
11X-3, 102–104	301.33	48.90	95.68	1.41	0.72	2.23	67.55	2.08	1.37	0.01	0.969	
19X-1, 102–104	321.55	44.15	79.06	1.51	0.84	2.40	64.92	1.85	1.58	0.00	1.049	1.062
19X-2, 102–104	323.05	41.59	71.21	1.54	0.90	2.42	62.71	1.68	1.66	0.00	1.074	
19X-3, 82–92	324.36	40.61	68.38	1.57	0.93	2.48	62.34	1.66	1.57	0.83	0.998	
20X-1, 82–92	327.10	39.95	66.52	1.60	0.96	2.56	62.45	1.66	1.59	0.00	0.995	1.009
20X-2, 72–82	327.99	39.47	65.21	1.57	0.95	2.40	60.41	1.53	1.60	0.01	1.022	
21X-1, 102–104	330.30	43.29	76.33	1.51	0.86	2.38	63.99	1.78	1.60	0.02	1.058	1.017
21X-2, 102–104	331.85	42.87	75.04	1.54	0.88	2.49	64.63	1.83	1.51	0.01	0.977	
22X-1, 60–62	339.60	41.92	72.18	1.53	0.89	2.39	62.75	1.68	1.64	0.00	1.071	NA
23X-1, 70–72	345.31	36.47	57.41	1.61	1.02	2.39	57.23	1.34	1.65	0.01	1.029	NA
27X-1, 110–112	368.50	31.90	46.84	1.74	1.18	2.59	54.21	1.18	1.84	0.00	1.059	1.037
27X-2, 100–102	369.90	29.14	41.13	1.78	1.26	2.57	50.79	1.03	1.84	0.00	1.032	
27X-3, 102–104	371.42	26.53	36.12	1.89	1.39	2.71	48.87	0.96	1.92	0.00	1.020	
28X-1, 102–104	372.82	27.29	37.54	1.86	1.35	2.69	49.67	0.99	2.01	0.00	1.079	1.045
28X-2, 102–104	374.32	25.38	34.01	1.91	1.42	2.69	47.23	0.89	1.96	0.00	1.031	
28X-3, 102–104	375.85	28.39	39.65	1.87	1.34	2.80	51.98	1.08	1.95	0.01	1.041	
28X-4, 42–44	376.75	24.78	32.94	1.90	1.43	2.65	45.98	0.85	1.96	0.01	1.030	
302-M0004C-												
1H-1, 100–102	1.00	37.13	59.07	1.68	1.06	2.71	60.96	1.56	1.61	0.00	0.958	0.971
1H-2, 100–102	2.51	38.73	63.20	1.66	1.01	2.71	62.60	1.67	1.57	0.01	0.948	
1H-3, 40–42	3.42	31.28	45.53	1.79	1.23	2.72	54.69	1.21	1.80	0.00	1.007	
2H-1, 100–102	5.00	30.06	42.97	1.81	1.27	2.71	53.19	1.14	1.91	0.00	1.052	1.051
2H-2, 100–102	6.50	38.88	63.61	1.65	1.01	2.72	62.82	1.69	1.74	0.00	1.052	
2H-3, 100–102	8.01	29.85	42.55	1.83	1.28	2.74	53.23	1.14	1.92	0.01	1.049	
3H-1, 100–102	9.95	33.16	49.61	1.76	1.18	2.74	57.03	1.33	1.80	0.00	1.021	1.033
3H-2, 100–102	11.46	34.79	53.35	1.73	1.13	2.73	58.73	1.42	1.78	0.01	1.031	
3H-3, 100–102	12.97	31.81	46.65	1.78	1.21	2.72	55.33	1.24	1.86	0.00	1.046	
4H-1, 70–72	14.67	35.22	54.36	1.72	1.11	2.72	59.06	1.44	1.86	0.00	1.081	1.070
4H-2, 100–102	16.47	30.90	44.71	1.80	1.24	2.72	54.31	1.19	1.91	0.00	1.059	
5X-1, 50–52	19.07	33.47	50.32	1.75	1.17	2.73	57.31	1.34	1.75	0.01	0.998	NA

Notes: Crossed out text corresponds to moisture and density (MAD) measurements not used in determination of correction factors because either no depth-equivalent multisensor core logger (MSCL) data were available or the MAD measurement was deemed to be nonrepresentative. NA = not applicable.



**Table T2.** Correction factors used to correct MSCL  $\rho_B$  from each core.

Core	Lith. unit	Average correction	Core	Lith. unit	Average correction			
<b>302-</b>								
M0002A-1X	1.1	<b>0.99</b>	M0002A-51X	2	<b>1.03</b>			
M0002A-2X	1.1	<b>0.99</b>	M0002A-52X	2	<b>1.03</b>			
M0002A-3X	1.2	<b>1.04</b>	M0002A-53X	2	1.00			
M0002A-4X	1.2	<b>1.04</b>	M0002A-54X	2	<b>1.03</b>			
M0002A-5X	1.3	<b>1.05</b>	M0002A-55X	2	1.00			
M0002A-6X	1.3	1.10	M0002A-56X	2	1.03			
M0002A-7X	1.3	1.07	M0002A-57X	2	1.01			
M0002A-8X	1.3	1.07	M0002A-58X	2	1.00			
M0002A-9X	1.3	1.09	M0002A-59X	2	<b>1.03</b>			
M0002A-10X	1.3	1.08	M0002A-60X	2	1.02			
M0002A-11X	1.3	1.04	M0002A-61X	2	1.04			
M0002A-12X	1.3	1.05	M0002A-62X	2	1.16			
M0002A-13X	1.3	<b>1.05</b>	<b>302-</b>					
M0002A-14X	1.3	1.03	M0004A-1H	1.2	1.04			
M0002A-15X	1.3	0.99	M0004A-2X	1.2	1.02			
M0002A-16X	1.3	1.05	M0004A-3X	1.3	1.08			
M0002A-17X	1.3	1.02	M0004A-4X	2	<b>1.03</b>			
M0002A-18X	1.3	1.07	M0004A-5X	2	<b>1.03</b>			
M0002A-19X	1.3	<b>1.05</b>	M0004A-6X	2	1.05			
M0002A-20X	1.3	1.09	M0004A-7X	2	1.04			
M0002A-21X	1.3	1.05	M0004A-8X	2	<b>1.03</b>			
M0002A-22X	1.3	<b>1.05</b>	M0004A-9X	2	<b>1.03</b>			
M0002A-23X	1.3	0.99	M0004A-10X	2	1.04			
M0002A-24X	1.3	1.02	M0004A-11X	2	0.98			
M0002A-25X	1.3	1.02	M0004A-15X	2	<b>1.03</b>			
M0002A-26X	1.3	<b>1.05</b>	M0004A-18X	3	<b>1.04</b>			
M0002A-27X	1.3	1.01	M0004A-10X	3	1.06			
M0002A-28X	1.3	<b>1.05</b>	M0004A-20X	3	1.01			
M0002A-29X	1.3	1.04	M0004A-21X	3	1.02			
M0002A-30X	1.3	1.00	M0004A-22X	3	1.07			
M0002A-31X	1.3	<b>1.05</b>	M0004A-23X	3	<b>1.04</b>			
M0002A-32X	1.3	1.07	M0004A-27X	3	1.05			
M0002A-33X	1.3	1.02	M0004A-28X	3	<b>1.04</b>			
M0002A-34X	1.3	1.06	M0004A-29X	3	<b>1.04</b>			
M0002A-35X	1.3	1.00	M0004A-30X	3	<b>1.04</b>			
M0002A-36X	1.3	<b>1.05</b>	M0004A-32X	3	<b>1.04</b>			
M0002A-37X	1.3	1.01	M0004A-33X	3	<b>1.04</b>			
M0002A-38X	1.4	1.02	M0004A-34X	3	<b>1.04</b>			
M0002A-39X	1.4	1.01	M0004A-35X	3	<b>1.04</b>			
M0002A-40X	1.4	<b>1.03</b>	<b>302-</b>					
M0002A-41X	1.4	<b>1.03</b>	M0004C-1H	1.1	0.97			
M0002A-42X	1.4	1.05	M0004C-2H	1.1	1.05			
M0002A-43X	1.4	1.03	M0004C-3H	1.2	1.03			
M0002A-44X	1.5	1.02	M0004C-4H	1.2	1.07			
M0002A-45X	1.5	<b>1.03</b>	M0004C-5X	1.2	1.00			
M0002A-46X	1.6	1.09	M0004C-6X	1.2	1.04			
M0002A-47X	1.6	1.02	M0004C-8X	1.3	1.04			
M0002A-48X	1.6	1.00	M0004C-9X	1.3	<b>1.04</b>			
M0002A-49X	1.6	1.03						
M0002A-50X	1.6	<b>1.03</b>						

Note: Bold text denotes cores for which the average correction factor from the corresponding lithologic unit/subunit was used.



**Table T3.** Average correction factors and grain density for lithologic units/subunits.

Unit	Grain density (g/cm <sup>3</sup> )		N	Density correction factor	
	Average	SD		cf*	SD
1	2.72	0.07	123	1.038	0.039
1.1	2.71	0.00	4	0.991	0.048
1.2	2.71	0.08	14	1.039	0.032
1.3	2.72	0.03	74	1.043	0.037
1.4	2.74	0.01	14	1.026	0.027
1.5	2.61	0.07	5	1.032	0.064
1.6	2.81	0.16	12	1.025	0.042
2	2.24	0.07	38	1.033	0.048
3	2.54	0.14	16	1.038	0.029
3a	2.43	0.06	9		
3b	2.67	0.08	7		
All units	2.60	0.21	177	1.037	0.040

Notes: Italicized text represents values for the two petrologic subdivisions of lithologic Unit 3 made in this paper. N = number of observations. SD = standard deviation. \* = see Equation 5 for cf calculation.

**Table T4.** Corrected MSCL  $\rho_B$  data and derived  $\rho_D$  and  $\phi$  records.

Site	Hole	Core	Type	Number	Depth (cm)	Depth (mbsf)	Liner thickness (cm)	Bulk density (g/cm <sup>3</sup> )	Lith. unit	Correction factor (cf)	Corrected density (g/cm <sup>3</sup> )	Porosity (%)	Void ratio
2	A	1	X	1	8.0	0.08	6.59	1.26	1.1	0.991	1.27	85.72	6.00
2	A	1	X	1	10.0	0.10	6.58	1.36	1.1	0.991	1.37	80.19	4.05
2	A	1	X	1	12.0	0.12	6.57	1.48	1.1	0.991	1.49	73.33	2.75
2	A	1	X	1	14.0	0.14	6.56	1.51	1.1	0.991	1.52	71.44	2.50
2	A	1	X	1	16.0	0.16	6.56	1.59	1.1	0.991	1.60	67.13	2.04
2	A	1	X	1	18.0	0.18	6.55	1.70	1.1	0.991	1.72	60.35	1.52
2	A	1	X	1	20.0	0.20	6.55	1.79	1.1	0.991	1.81	55.24	1.23
2	A	1	X	1	22.0	0.22	6.54	1.70	1.1	0.991	1.72	60.34	1.52
2	A	1	X	1	24.0	0.24	6.54	1.76	1.1	0.991	1.77	57.13	1.33
2	A	1	X	1	26.0	0.26	6.53	1.80	1.1	0.991	1.82	54.55	1.20
2	A	1	X	1	28.0	0.28	6.53	1.76	1.1	0.991	1.78	56.97	1.32
2	A	1	X	1	30.0	0.30	6.53	1.76	1.1	0.991	1.78	57.09	1.33
2	A	1	X	1	32.0	0.32	6.53	1.81	1.1	0.991	1.83	54.03	1.18
2	A	1	X	1	34.0	0.34	6.53	1.58	1.1	0.991	1.60	67.28	2.06
2	A	1	X	1	36.0	0.36	6.53	1.66	1.1	0.991	1.67	63.05	1.71
2	A	1	X	1	38.0	0.38	6.53	1.83	1.1	0.991	1.85	52.81	1.12
2	A	1	X	1	40.0	0.40	6.53	1.91	1.1	0.991	1.93	48.48	0.94
2	A	1	X	1	42.0	0.42	6.53	1.79	1.1	0.991	1.80	55.65	1.25
2	A	1	X	1	44.0	0.44	6.53	1.58	1.1	0.991	1.59	67.45	2.07
2	A	1	X	1	46.0	0.46	6.53	1.62	1.1	0.991	1.64	65.03	1.86
2	A	1	X	1	48.0	0.48	6.53	1.77	1.1	0.991	1.78	56.82	1.32
2	A	1	X	1	50.0	0.50	6.52	1.73	1.1	0.991	1.74	58.99	1.44
2	A	1	X	1	52.0	0.52	6.52	1.72	1.1	0.991	1.74	59.17	1.45
2	A	1	X	1	54.0	0.54	6.52	1.89	1.1	0.991	1.91	49.49	0.98
2	A	1	X	1	56.0	0.56	6.52	1.90	1.1	0.991	1.92	48.92	0.96
2	A	1	X	1	58.0	0.58	6.52	1.91	1.1	0.991	1.92	48.75	0.95
2	A	1	X	1	60.0	0.60	6.52	1.71	1.1	0.991	1.73	59.80	1.49
2	A	1	X	1	62.0	0.62	6.52	1.74	1.1	0.991	1.76	58.23	1.39
2	A	1	X	1	64.0	0.64	6.53	1.73	1.1	0.991	1.75	58.79	1.43
2	A	1	X	1	66.0	0.66	6.53	1.78	1.1	0.991	1.79	56.20	1.28
2	A	1	X	1	68.0	0.68	6.53	1.83	1.1	0.991	1.84	53.15	1.13
2	A	1	X	1	70.0	0.70	6.53	1.81	1.1	0.991	1.82	54.41	1.19
2	A	1	X	1	72.0	0.72	6.53	1.72	1.1	0.991	1.74	59.25	1.45
2	A	1	X	1	74.0	0.74	6.53	1.70	1.1	0.991	1.72	60.29	1.52
2	A	1	X	1	76.0	0.76	6.53	1.69	1.1	0.991	1.71	61.12	1.57
2	A	1	X	1	78.0	0.78	6.53	1.68	1.1	0.991	1.69	61.77	1.62
2	A	1	X	1	80.0	0.80	6.52	1.70	1.1	0.991	1.72	60.50	1.53
2	A	1	X	1	82.0	0.82	6.52	1.77	1.1	0.991	1.78	56.72	1.31
2	A	1	X	1	84.0	0.84	6.52	1.85	1.1	0.991	1.87	51.65	1.07
2	A	1	X	1	86.0	0.86	6.52	1.93	1.1	0.991	1.95	47.26	0.90
2	A	1	X	1	88.0	0.88	6.51	1.92	1.1	0.991	1.94	47.86	0.92
2	A	1	X	1	90.0	0.90	6.51	1.92	1.1	0.991	1.94	47.87	0.92
2	A	1	X	1	92.0	0.92	6.51	1.90	1.1	0.991	1.91	49.23	0.97
2	A	1	X	1	94.0	0.94	6.51	1.91	1.1	0.991	1.92	48.66	0.95
2	A	1	X	1	96.0	0.96	6.51	1.83	1.1	0.991	1.84	53.30	1.14
2	A	1	X	1	98.0	0.98	6.50	1.87	1.1	0.991	1.88	51.01	1.04
2	A	1	X	1	100.0	1.00	6.50	1.88	1.1	0.991	1.90	49.91	1.00
2	A	1	X	1	102.0	1.02	6.51	1.91	1.1	0.991	1.93	48.33	0.94
2	A	1	X	1	104.0	1.04	6.51	1.97	1.1	0.991	1.98	45.26	0.83
2	A	1	X	1	106.0	1.06	6.51	1.99	1.1	0.991	2.00	44.00	0.79
2	A	1	X	1	108.0	1.08	6.51	2.00	1.1	0.991	2.02	43.34	0.76
2	A	1	X	1	110.0	1.10	6.51	1.99	1.1	0.991	2.00	44.11	0.79
2	A	1	X	1	112.0	1.12	6.51	1.98	1.1	0.991	2.00	44.20	0.79
2	A	1	X	1	114.0	1.14	6.52	1.96	1.1	0.991	1.98	45.57	0.84
2	A	2	X	1	4.0	1.54	6.62	1.70	1.1	0.991	1.71	60.58	1.54
2	A	2	X	1	6.0	1.56	6.62	1.78	1.1	0.991	1.79	56.22	1.28
2	A	2	X	1	8.0	1.58	6.61	1.82	1.1	0.991	1.84	53.64	1.16
2	A	2	X	1	10.0	1.60	6.60	1.82	1.1	0.991	1.84	53.54	1.15
2	A	2	X	1	12.0	1.62	6.58	1.80	1.1	0.991	1.82	54.59	1.20
2	A	2	X	1	14.0	1.64	6.58	1.79	1.1	0.991	1.80	55.42	1.24
2	A	2	X	1	16.0	1.66	6.57	1.82	1.1	0.991	1.84	53.44	1.15
2	A	2	X	1	18.0	1.68	6.56	1.76	1.1	0.991	1.77	57.16	1.33
2	A	2	X	1	20.0	1.70	6.56	1.83	1.1	0.991	1.85	53.02	1.13

Notes: Only a portion of this table appears here. The complete table is available in ASCII and Microsoft Excel format in "Supplementary Material."

